# The Ouzo effect: A tool to elaborate high-payload nanocapsules

Clément Goubault, Flavien Sciortino, Olivier Mongin, Ulrich Jarry, Mégane Bostoen, Hélène Jakobczyk, Agnès Burel, Stéphanie Dutertre, Marie-Bérangère Troadec, Myrtil L. Kahn, et al.

# The Ouzo effect: a tool to elaborate high-payload nanocapsules

Clément Goubault[1], Flavien Sciortino[1], Olivier Mongin[1], Ulrich Jarry[2], Mégane Bostoen[2], Hélène Jakobczyk[3], Agnès Burel[4], Stéphanie Dutertre[4], Marie-Bérangère Troadec[5,6], Myrtil L. Kahn[7], Soizic Chevance[1], Fabienne Gauffre[1,*] fabienne.gauffre@univ-rennes1.fr

Corresponding author*:

[1]Univ Rennes, CNRS, ISCR-UMR6226, F-35000 Rennes, France
[2]Univ Rennes, CNRS, INSERM, BIOSIT - UMS 3480, LabCom Oncotrial, Biotrial Pharmacology, F-35000 Rennes, France
[3]Univ Rennes, CNRS, IGDR - UMR 6290, F-35000 Rennes, France
[4]Univ Rennes, CNRS, INSERM, BIOSIT - UMS 3480, US_S 018, MRic, F-35000 Rennes, France
[5]Univ Brest, INSERM, EFS, UMR 1078, GGB, F-29200 Brest, France
[6]CHRU Brest, laboratoire de génétique chromosomique, Brest, France
[7]LCC, CNRS, F-31000 Toulouse, France

*Corresponding author.

**Abstract**

We investigate the encapsulation in Hybridosomes®, a type of capsules unique regarding their structure and method of elaboration. Hybridosomes®, are made of a single shell of nanoparticles (~5 nm) crosslinked with a polymer and are easily obtained *via* spontaneous emulsification in a ternary mixture THF/water/butylated hydroxytoluene (BHT). Our main finding is that an exceptionally high concentration of a hydrophobic model dye can be loaded in the hybridosomes®, up to 0.35 mol.L$^{-1}$ or equivalently 170 g.L$^{-1}$ or 450 000 molecules/capsule. The detailed investigation of the encapsulation mechanism shows that the dye concentrates in the droplets during the emulsification step simultaneously with capsule formation. Then it precipitates inside the capsules during the course of solvent evaporation. *In vitro* fluorescence measurements show that the nano-precipitated cargo can be transferred from the core of the hybridosomes® to the membrane of liposomes. *In vivo* studies suggest that the dye diffuses through the body during several days. The released dye tends to accumulate in body-fat, while the metal-core nanoparticles remained trapped into the liver and the spleen macrophages.

**Keywords:** Hybridosomes®; encapsulation; nanoprecipitation, Ouzo effect, hydrophobic cargo

## Introduction

Encapsulation is a major issue in nanomedicine for the delivery of toxic, unstable or poorly soluble drugs but also for the food and cosmetic industries [1–6]. A large variety of encapsulation systems are available, including polymer nanoparticles (NP), micelles, liposomes and polymersomes, silica NP, nanogels and solid-lipid NP, to name only a few [7–14]. The selection of the encapsulation technology is dictated both by the application and by the properties of the cargo. In particular, the hydrophilic or hydrophobic nature of the cargo is a determining factor. Thus, hydrophobic ingredients will most often be encapsulated in the hydrophobic core of solid-lipid NP or of polymer micelles, whereas nanogels or liposomes will be preferred for hydrophilic ones. Besides, for any medical or biotechnology applications, the size needs to be precisely controlled as a key factor for

the biodistribution of the nanocarrier [15–17]. Indeed, size strongly influences the adsorption of plasma proteins (opsonins) which triggers the clearance from the bloodstream. Renal filtration and accumulation in the liver also depend on the NP size. Thus, it is generally admitted that particles with diameter below 5 nm are rapidly evacuated via renal clearance, whereas partide larger than 10 nm are captured by phagocytic cells, unless they are rendered stealthy by surface modification [15,17,18].

Whilst most studies have focused on the pharmacokinetics and therapeutic efficacy of encapsulated drugs, strategies to improve loading have been overlooked. To date, this remains one of the challenging issues of drug encapsulation. Indeed, achieving a very high encapsulation efficiency reduces losses of active ingredients. In addition, the more the carrier is loaded, the lower the level of excipient relative to the active molecules. In the case of liposomes, the simplest approach for drug encapsulation is passive loading: the liposomes are formed from a lipid film by rehydration in a buffer containing the drug to encapsulate. Therefore, the inner and outer drug concentrations are similar, and inherently limited by the solubility of the drug in the buffer. Whilst relatively convenient and easy, this method suffers from low encapsulation efficacy and high levels of non-encapsulated drugs, which need to be eliminated. The *active* (or *remote*) loading driven by a transmembrane pH-gradient has successfully enabled the loading of large amounts of drugs. Thus Doxil®, which was the first liposomal formulation approved by FDA in 1995, is an emblematic example of the use of active loading. The load reaches ca 10 000 doxorubicin molecules per liposome (typically 0.05-0.1 mol.$L^{-1}$), in the form of its ammonium salt [19–21]. The encapsulation mechanism is based on a transmembrane pH-gradient coupled to the precipitation of the ammonium salt in the core of the liposome. The precipitation produces a sink effect, which drives the doxorubicin inward [20,22]. Interestingly, the low solubility of the salt helps slowing down the release of the drug from the liposome. Active loading has been extended to a few other drugs including ciprofloxacin, vincristine, topotecan and irinotecan using ammonium sulfate, citric acid, calcium acetate, phosphate or EDTA gradients [22]. Despite these undeniable successes, the active loading method remains complex to implement. In addition, it is limited to a relatively low number of amphiphilic and acidic (or basic) drugs, and cannot be applied to hydrophobic drugs.

In contrast, the co-precipitation of polymers and drugs is a straightforward strategy to encapsulate hydrophobic drugs into polymer NP [23]. In practice, the polymer and hydrophobic solute are dissolved into an organic solvent miscible with water, typically acetone, ethanol or tetrahydrofuran (THF). This solution is then rapidly mixed with a large amount of water to induce nanoprecipitation. It was shown that under appropriate conditions this process can generate polymer/drug particles in the 50-300 nm range, with a very narrow size-dispersity [9,24]. However, the main drawback of co-precipitation in the form of particles is the large amount of excipient, generally biodegradable polymers such as poly(lactic acid) and poly-(*iso*-hexylcyanoacrylate) [8] , relative to the encapsulated drug. For this reason, a process leading to pure drug nanoprecipitation in a capsule would be more advantageous, provided that the process remains simple to implement. Interestingly, the “Ouzo effect”, a process related to nanoprecipitation, can produce such capsules. The Ouzo effect occurs in ternary systems consisting of a water-miscible solvent, water, and a low amount of oil. Beyond a certain amount of water, oil-rich droplets separate from the continuous phase. This phenomenon is responsible for the appearance of the turbidity in the well-known Greek beverage and its analogues, such as Pastis or Raki [25–29]. More generally, different situations are grouped under the term “Ouzo effect”. Indeed, depending on the solvent/water ratio, these systems can form either a

thermodynamically stable micro-emulsion (SFME for surfactant free micro-emulsion) or a metastable phase (the "Ouzo domain") with oil droplets coalescing more or less rapidly. In the SFME domain, the droplets have a submicronic size with a very narrow polydispersity. Interestingly, it was shown by Ganachaud *et al.* that the droplets formed in the SFME domain can be used as templates to elaborate capsules of polymer [30] or fluorescent organic nanoparticles [31].

More recently, our group reported the use of the Ouzo effect to form hybrid inorganic-NP/polymer capsules, named hybridosomes® [32–34]. The procedure of elaboration of the hybridosomes® *via* the Ouzo effect is summarized in Figure 1[32]. Hydrophobic NP are first suspended in THF (as the water-miscible solvent) containing a preservative (Butylated Hydroxytoluene, BHT, as the lipophilic compound). Then, a large amount of water (typically 0.7-0.9 in terms of volumic fraction) is added to generate supersaturation of the oil and nucleation of droplets. Simultaneously to droplet formation, the NP which are also hydrophobic, become incompatible with the water-rich solvent, and precipitate at the interface of the Ouzo droplets. Although this process may seem similar to Pickering emulsions, we wish to underline here an important difference. In the case of Pickering emulsions, the partides are adsorbed at the interface, in equilibrium with the bulk phase, with an adsorption energy proportional to the square of the particle radius [35,36]. In practice, nanoparticles are only very weakly adsorbed, which severely limits their efficiency for the stabilization of emulsions. Here, in the contrary, the nanoparticles are irreversibly precipitated at the droplet surface. It is interesting to note that if a low amount of water is added (typically < 0.5 in the case of THF) the NP precipitates out of the ouzo domain, while the drops are not formed [32]. We then observe a macroscopic precipitate and not the formation of capsules. For this reason, it is necessary to add a large fraction of water quickly. Finally, we crosslink the NP with a polymer, which provides mechanical robustness to the capsules, enabling the replacement of the solvent core with water, either by evaporation or dialysis.

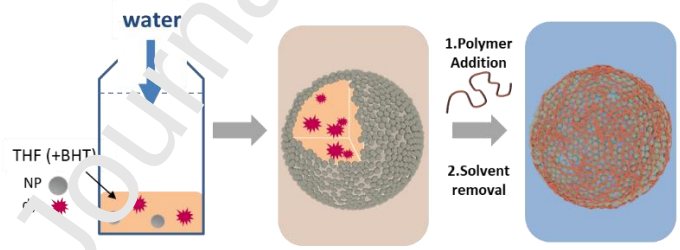


Figure 1 – Schematic representation of the process of elaboration of the Hybridosomes® *via* the nanoprecipitation of hydrophobic NP at the surface of Ouzo droplets. Water is rapidly added to a THF solution containing hydrophobic NP (here, Superparamagnetic Iron Oxide NP, coated with octylamine) and BHT (here THF 25%/water 75%/BHT<0.01%). Ouzo droplets form and the NP cover their surface. Then, a polymer (PAA-*b*-PEG) is added to crosslink the NP. After removal of the solvent (evaporation or dialysis), the core is substituted with water.

Herein, we hypothesized that the specific mechanism of capsule formation *via* the Ouzo effect is intrinsically very efficient for encapsulation. Using a fluorescent BODIPY dye with different spectral characteristics in the solid and liquid states[37], we investigated in great details the physical state of the dye in the course of its encapsulation in hybridosomes® and determined the encapsulation efficiency and the internal payload. Besides, we studied the release of the cargo, *in vitro* and *in vivo,* using luminescence measurements and demonstrated that the dye is able to diffuse into cells cytoplasm and distributes through the body after intravenous injection.

**Results & Discussion:**

## 1. Encapsulation

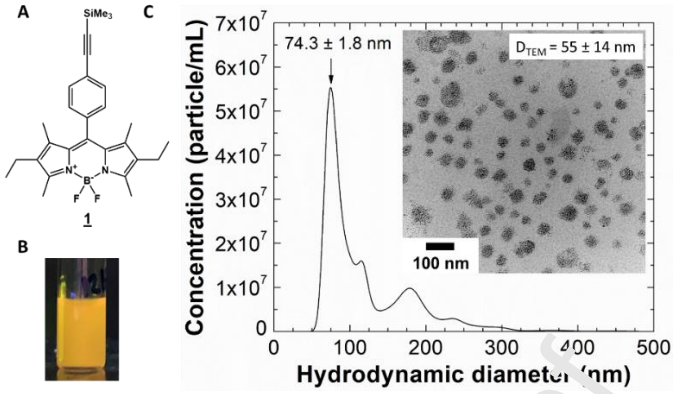


Figure 2 – (A) Structure of the BODIPY **1**. (B-C) Characterization of a suspension of BODIPY-loaded hybridosomes® ([BODIPY] = 50 mmol.L$^{-1}$) (B) Photograph under UV-irradiation ($\lambda_{exc}$ = 365 nm). (C) Size distribution using Nanoparticle Tracking Analysis (NTA) and Transmission Electron Microscopy (TEM) (inset).

*A straightforward encapsulation procedure.* To achieve encapsulation, the target compound is simply added to the organic phase beforehand as shown in Figure 1[37]. In the present work, we selected the fluorescent BODIPY dye **1** (Figure 1A), synthesized in the laboratory, as a model compound to investigate the encapsulation. Indeed, this dye is poorly soluble in water (*see SI section A*), which is an important factor for its sequestration in the Ouzo droplets. Moreover, in contrast to most dyes, the solid form of **1** is also significantly emissive with a red shift compared to the soluble form, which is useful to probe its physical state and image dye-loaded hybridosomes®. To facilitate the purification step, we prepared the hybridosomes® from superparamagnetic iron oxide NP (SPION, 5 nm) [38] coated with an oleylamine ligand. Then, the NP shell was crosslinked by a poly(ethylene glycol)$_{2k}$-*b*-poly(acrylic)$_{7k}$ diblock copolymer (PEG-PAA). As shown in our previous work, these hybridosomes® (SPION@PEG-PAA hybridosomes®) can be easily separated from the bulk using a permanent magnet. In contrast to other separation methods such as centrifugation and steric exclusion, magnetic separation allows to selectively attract the magnetic hybridosomes®, leaving aside non-encapsulated nanoprecipitated dye, if any.

Regarding the Ouzo system, we selected a THF/water mixture (25/75). Indeed, THF is a good solvent for both the alkylamine-coated SPION and **1**. No oil is added to the system, as standard commercial THF already contains traces of an hydrophobic antioxidant preservative, butylated hydroxytoluene (BHT ~ 320 mg.L$^{-1}$; water solubility ~ 0.6 mg.L$^{-1}$ [39]; LogP = 5.10 [40]) which can play the role of the oil in the Ouzo emulsion. Indeed, previous work has shown that BHT was responsible for the formation of droplets of the order of a few hundreds of nanometers in THF/water mixtures [41]. To confirm this result in our own conditions, dynamic light scattering (DLS) measurements of THF/water mixture (25/75) were performed (Figure S 1). Two types of THF were compared: the BHT-containing THF used in our preparations and the preservative-free THF. It appears clearly that the presence of BHT is necessary to observe such mesoscopic structures (with the principal mode for the mean hydrodynamic diameter at 190 nm). Both BODIPY and BHT can participate in the formation of Ouzo droplets. According to our measurements, BHT is present at a concentration of 0.36 mmol.L$^{-1}$ in the initial THF/water 25/75 mixture. As for BODIPY **1**, its concentration varies between 5 and 150 µmol.L$^{-}$

[1]. Calculation of the solubility of these two compounds in THF/water mixtures, using the thermodynamic calculation software COSMO-RS (**Error! Reference source not found.**) [42], shows that **1** is much less soluble than BHT, by two or three orders of magnitude. Both concentrations are close to or beyond the solubility limits in the THF/water (25/75) continuous phase (1.3 $mmol.L^{-1}$ and 1.5 $\mu mol.L^{-1}$ for BHT and **1**, respectively). These calculations explain the presence of droplets observed in the mixture of water and commercial THF. They also suggest that under these conditions of concentration, BODIPY will be found mainly in the dispersed phase.

Dye-loaded hybridosomes® were prepared according to these conditions. Figure 2 shows a photograph of a suspension of dye-loaded hybridosomes® under UV-irradiation ($\lambda_{exc}$ = 365 nm), as well as size measurements using transmission electron microscopy (TEM) (mean diameter: 55 ± 14 nm) and nanopartide tracking analysis (NTA) (hydrodynamic diameter main mode: 74.3 ± 1.8 nm). The absorbance spectra of **1** under its soluble and nanoprecipitated are displayed in **Error! Reference source not found.**.

*Investigation of nanoprecipitation.* We first investigated the behavior of the dye during nanoprecipitation, in the absence of NP. Figure 3 shows the emission spectra of BODIPY **1**, in THF and in the THF/water mixture (25/75). Both spectra are very similar, with a main emission band at 538 nm suggesting that the dye is dissolved in both cases. However, at this point we do not know whether the dye is dissolved in the continuous phase (THF/water mixture) or in the Ouzo droplets. After total evaporation of THF and centrifugal purification, the emission spectrum of the resuspended pellet exhibits two broad bands at 555 and 620 nm. The red shift of the main emission (from 538 to 555 nm) and the emergence of a second emission transition at lower energy are attributed to a nanodispersed form of **1** [43,44]. The presence of a nanodispersed form is confirmed by NTA which shows a population of 132 ± 1 nm (**Error! Reference source not found.**).

In a second time, we measured the emission spectra of **1** when encapsulated in the hybridosomes®. In this case, the feature of the emission is very similar to that of the nanoprecipitated form, suggesting that the encapsulated dye is also a nanoprecipitate. Nevertheless, the peak at 555 nm seems to be more predominant compared to the nanodispersed non-encapsulated form of BODIPY. This may be due to a fraction of **1** solubilized in the PEG block of PEG-PAA. Note that both the nanoprecipitated and encapsulated form of BODIPY show lower emission intensity (~ 1/10) than the soluble form. At this point, our results clarify an important issue: the dye is mostly localized in the droplet. If this was not the case, it would nanoprecipitate outside of the hybridosomes® during the evaporation of the solvent.

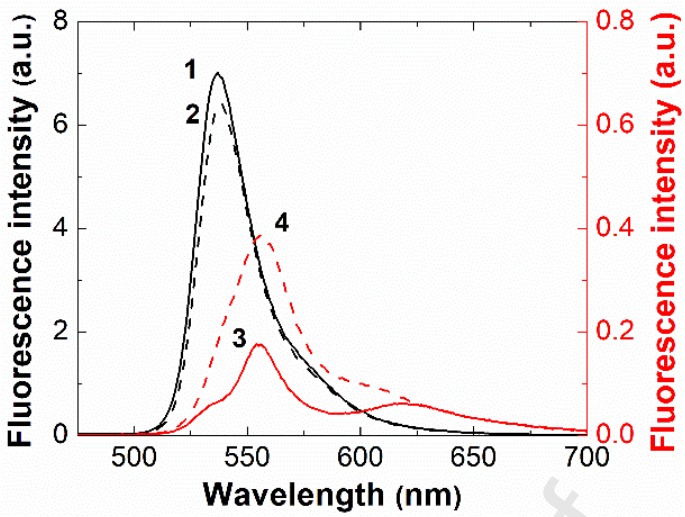


Figure 3 – Fluorescence emission spectra of BODIPY **1** at different steps of the process ($\lambda_{exc}$ = 400 nm). 1) Dissolved BODIPY in THF (plain black line); 2) BODIPY in THF/water (25/75) mixture (dashed black line); 3) Nanoprecipitated BODIPY (plain red line); 4) BODIPY encapsulated in PEG-PAA-stabilized iron oxide hybridosomes® (dashed red line).

*Quantitative evaluation of loading*. The efficiency of loading was characterized from the measurement of the absorbance of the dye in the hybridosomes® and in the supernatant after magnetic separation. Figure 4 shows both the *encapsulation yield* (defined as the amount of encapsulated dye over the total amount of dye) and the *internal concentration* in the hybridosomes® ($[BOD]_{in}$), for different total concentrations of dyes ($[BOD]_{tot}$). These are calculated from experimental values reported in **Error! Reference source not found.**. For all concentrations, a very high encapsulation yield was found (88 + 5%). Losses and variability can be partly attributed to the 2 steps of magnetic purifications. Interestingly, the internal concentration can be as high as 0.35 mol.L$^{-1}$ (or ~170 g.L$^{-1}$), which corresponds to ca 450 000 molecules/capsule. This is 2 to 50 times higher than values previously reported for Doxil® [19,20,45]. Changing the amount of SPION to prepare hybridosomes® does not modify the encapsulation yield (**Error! Reference source not found.**). This shows that there is no adsorption of the BODIPY on the NP surface. Indeed, if the encapsulation process was related to adsorption of the dye on the NP, there should be an increase of the encapsulated amount with the number of NP.

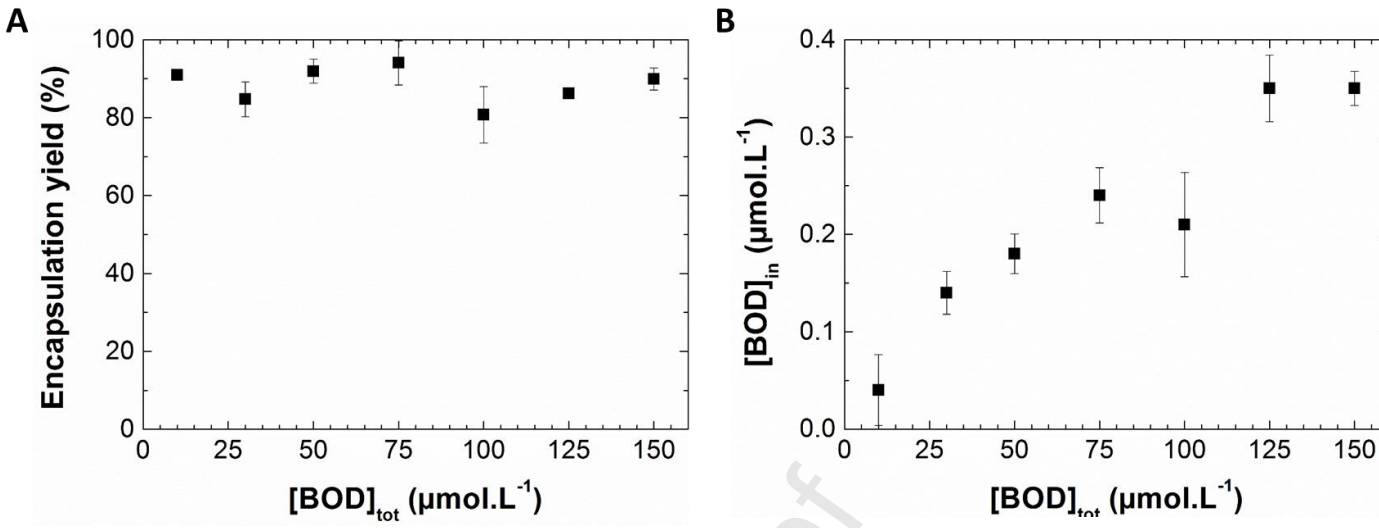


Figure 4 – (A) Encapsulation yield and (B) internal BODIPY concentration in hybridosomes® as a function of the total concentration of BODIPY.

Moreover, we investigated the influence of the total dye concentration on the nanoprecipitation in the absence of NP. In this case, water was rapidly added to THF solutions of **1** of various concentrations (10 – 150 µmol.L$^{-1}$), to reach the ratio THF/water (25/75). Then, THF was evaporated and the suspension centrifugated. The nanoprecipitation yield was determined from UV-visible measurements of the pellet after redispersion in THF (Figure 5). Very interestingly, the nanoprecipitation yield decreases with decreasing dye concentrations in the low initial concentrations range, which was not observed in the presence of hybridosomes®. More precisely, Figure 5 also shows that the concentration of dye recovered in the supernatant after centrifugation (empty squares) is ca 6 µmol.L$^{-1}$, whatever the total amount of dye in the mixture. The difference of behavior between the nanoprecipitation in solution and in the hybridosomes® is striking. For a detailed explanation, the reader is invited to refer to the SI section A "*Comparison of the nanoprecipitation vs encapsulation yield*". In brief, (i) in the case of nanoprecipitation without NP, the fraction of un-precipitated dye is related to the solid/liquid equilibrium of the dye, and directly corresponds to the solubility of the dye. (ii) In the case of hybridosomes®, the encapsulation yield corresponds to the fraction of dye nanoprecipitated in the hybridosomes® reported to the total amount of dye. It is found constant, as a result of the partitioning equilibrium of the dye between the continuous and the dispersed phase.

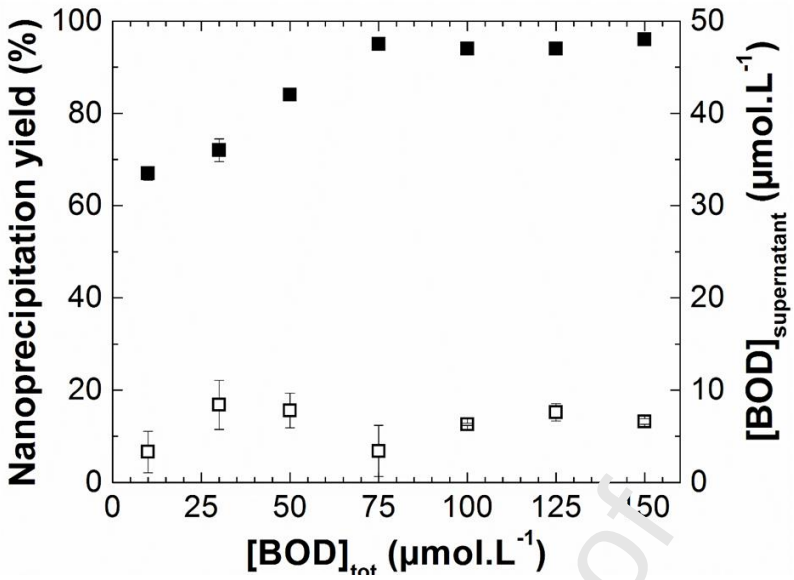


Figure 5 – Nanoprecipitation of BODIPY in water: nanoprecipitation yield (plain squares) and residual BODIPY concentration in the supernatant (empty squares).

### 2. *In vitro* and *in vivo* release

In a previous work, we demonstrated that hybridosomes® have a porous structure, with pores ~4 nm [33]. This should allow the leakage of encapsulated cargo. The water solubility of dye **1** being extremely low (ca $10^{-10}$ mol.L$^{-1}$), no release could be measured in pure water. Nevertheless, it is possible to investigate the release in a hydrophobic medium. To do this, we used a mixture of dye-loaded hybridosomes® and liposomes as a model of hydrophobic environment. In the presence of liposomes a dramatic enhancement of the luminescence is observed (**Error! Reference source not found.**), due to the transfer of the dye to the membrane of the liposomes. Figure 6a shows the kinetics of transfer of the dye from dye loaded hybridosomes® to the membrane of liposomes, for three concentrations of liposomes (2, 5, and 8 mg.mL$^{-1}$). The amount of transferred dye increases with time over more than one week (Figure 6b). In contrast, in pure fetal bovine serum, only a small fraction of the dye is solubilized, within the first day, most probably in proteins. Besides, the higher the lipid concentration, the higher the level of dye extracted. This indicates that the transfer of the dye from the hybridosomes® to the liposomes is driven by its solubility in the lipid membrane. As also shown in Figure 6, the solubilization kinetics of the nanoprecipitated dye is only slightly different from that of the hybridosome®-encapsulated dye, confirming the porous character of the hybridosomes®. These kinetics measurements can be satisfactorily fitted by the empirical Korsmeyer-Peppas equation $f = k.t^n$ [46–48], with n close to 0.5 (**Error! Reference source not found.** in SI section G), which strongly suggest that the limiting step is a diffusive process.

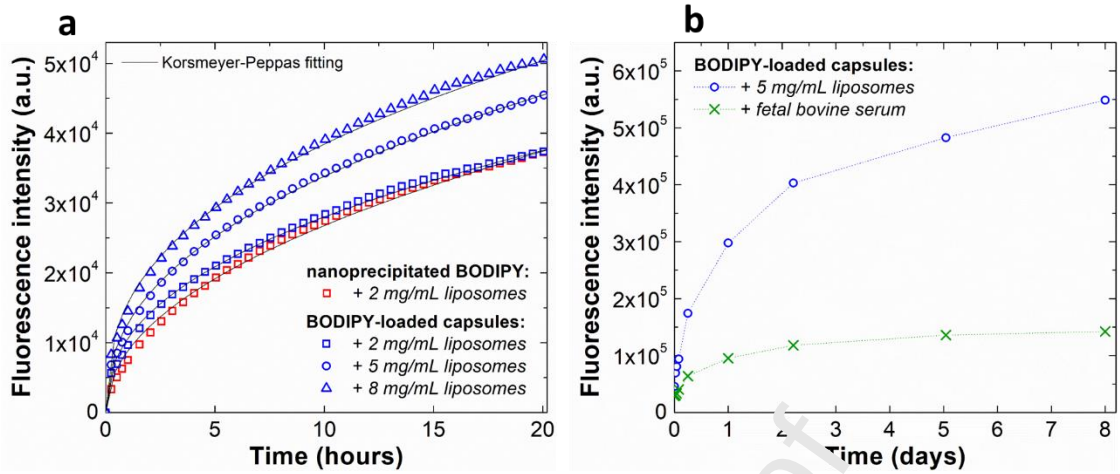


Figure 6 – Time-dependent release of BODIPY. (**a**) transfer from dye-loaded hybridosomes® to liposomes (lipid: 2 (□), 5 (○), 8 (△) mg.mL$^{-1}$) and (□): transfer from nanoprecipitated dye to liposomes (lipid: 2 mg.mL$^{-1}$); black lines: fit by empirical equation: $f=k.t^n$. **(b)**: long time scale transfer of **1** from dye-loaded hybridosomes® to liposomes (○, lipid: 5 mg/mL) and to fetal bovine serum (×).

In a second step, BODIPY-loaded hybridosomes® were incubated with malignant GL261 cells. This cell line is a frequently used murine glioma model and we considered it in the perspective of a future evaluation of hybridosomes® for treatment of glioblastoma [49]. Figure 7 shows confocal fluorescence images of dye-loaded hybridosomes® incubated with the cells, in the absence of any specific cell staining. Bright green spots are clearly visible inside the cells incubated with hybridosomes®. These are attributed to internalized BODIPY, probably in confined spaces such as lysosomes. In addition to these bright spots, the cytoplasm is rather uniformly stained with the dye, which obviously do not penetrate in the nucleus. Very interestingly, orange fluorescence is also visible and co-localized with the green fluorescence, validating the fact that is attributable to **1** which shows a characteristic dual green-orange emission as described in Figure 3. These results show that after 2 hours of incubation, the dye is partially released in the cytoplasm, and partially enclosed in intracellular compartments. Release of hydrophobic Bodipy dyes from NP into the cytosol of cells was previously reported and can occur even in the absence of uptake of the particles, through membrane mediated diffusion [50]. Note that internalization of nano-objects into cells depend both on the physico-chemical features of the nano-objects and on the cell types, phagocytic cells being more prone to internalization of particles over 50 nm [51]. In the present case, using iron oxide hybridosomes®, it is difficult to ascertain whether the hybridosomes® shells are taken up by the cells or not. However, experiments achieved using hybridosomes® made from fluorescent quantum dots suggest that they mostly remain at the membrane of the cells.

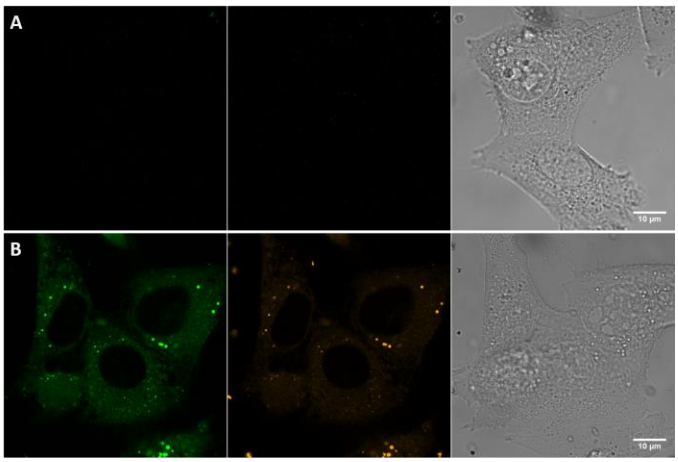


Figure 7 – Confocal fluorescence imaging of malignant GL261 cells (A) before and (B) after 2 h incubation with BODIPY-loaded hybridosomes®. From left to right, green fluorescence channel, orange fluorescence channel and transmitted light image.

Finally, dye-loaded hybridosomes® were injected into mice via two injection modes. Firstly, dye-loaded hybridosomes® were injected in matrigel® seeded with Nalm6 cells (Figure 8 A&B). Nalm6 cells are malignant lymphoblast cells, commonly used as model of acute lymphoblastic leukemia **[52]**. The green fluorescence was monitored over 2 weeks with a bioimager. Both the intensity (Figure 8 B) and the size of the fluorescent zone (Figure 8 A) increase over the duration of the study. Many nanomedicine studies have reported that, in contrast to molecular compounds, nanoparticles injected intratumorally remain close to the injection site because they are unable to migrate effectively through the extracellular matrix **[53–55]**. As we have just shown, the encapsulated dye can easily be released from hybridosomes® and incorporated into lipophilic reservoirs. In addition, green fluorescence is strongly attenuated through the body and can only be monitored when close to the surface. Therefore, the spreading of the fluorescent zone several millimeters away from the site of injection is most probably due to the release of the molecular dye and its accumulation into subcutaneous fat. Secondly, we performed an intravenous retro orbital injection (Figure 8 C&D). A green fluorescence appears gradually all over the mouse, with an increasing intensity over 5 days. This is also due to the accumulation of the dye in fatty tissues under the skin. Since previous experiments using MRI monitoring of SPION hybridosomes® evidenced that they were captured by liver and spleen macrophages within 30 min after injection [32], the present observations strongly support a release of the dye in the blood circulation.

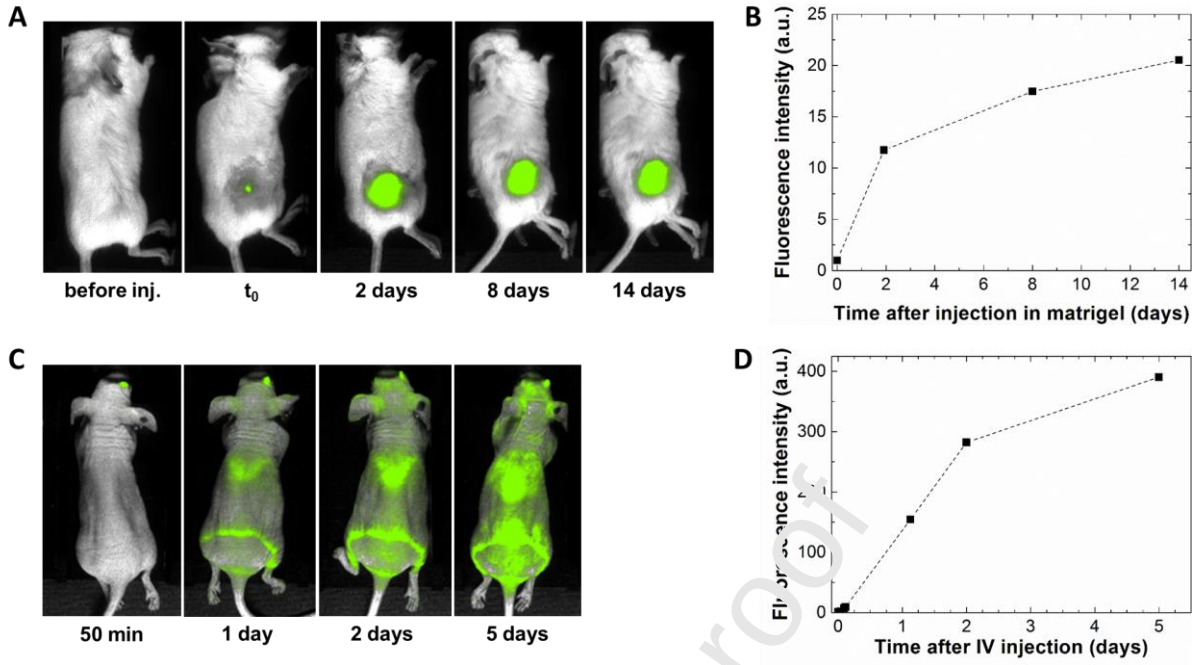


Figure 8 – (A) *In vivo* fluorescence bioimaging after injection of dye-loaded hybridosomes® in matrigel® containing Nalm6 cells; (B) Time evolution of the fluorescence intensity measured from (A). (C) *In vivo* fluorescence bioimaging after intravenous injection (retro-orbital vein). ($\lambda_{exc}$ = 488 nm ; $\lambda_{em}$ = 547 nm). (D) Time evolution of the fluorescence intensity measured from (A).

In order to complement these results, TEM was performed on sections of liver and spleen 24 hours after intravenous injection of hybridosomes® (Figure 9). As indicated by arrows, structures of ca 100 nm in diameter and presenting a strong contrast effect are detected in both the liver and the spleen. In accordance with our previous *in vivo* IVIRI experiments [32], it is reasonable to identify these structures as internalized hybridosomes®. In the liver, they were found in hepatocytes as well as in Kupffer cells (liver macrophages). Regarding the spleen, they were observed only in macrophage cells connected to endothelial cells and not in the red pulp lymphocytes cells. Within the cells, NP were mainly localized in vesicular compartments and not scattered in the cytoplasm, suggesting that the hybridosomes® were especially captured by the cellular degradation system. Since we have observed previously an accumulation of the hybridosomes® in the the liver in the course of the first hour after intravenous injection [32], it may seem surprising that the luminescence still increases after 5 days. The hypothesis of a rapid release in the blood pool, followed by a slow accumulation in the body fat may be ruled out. Indeed, our *in vitro* release experiment show a very limited transfer to serum albumin which suggests a low dissolution of the dye in the blood pool. In addition, molecular compounds released in the blood pool would be rapidly eliminated *via* renal excretion. A more likely mechanism would involve the Monocyte Phagocytic System (MPS)[56]. Indeed, it is widely reported in the case of nanoparticle formulation of hydrophobic drugs, that the particles are first uptaken by the MPS, and accumulates mainly in macrophages of the liver (Kupffer cells) and of the spleen [57,58]. Inside these cells they traffic through lysosomes. Due to their lipophilic character, they may pass the lysosomal membrane and finally exit the cell. This result in a pharmacokinetic profile with much prolonged $t_{1/2}$.

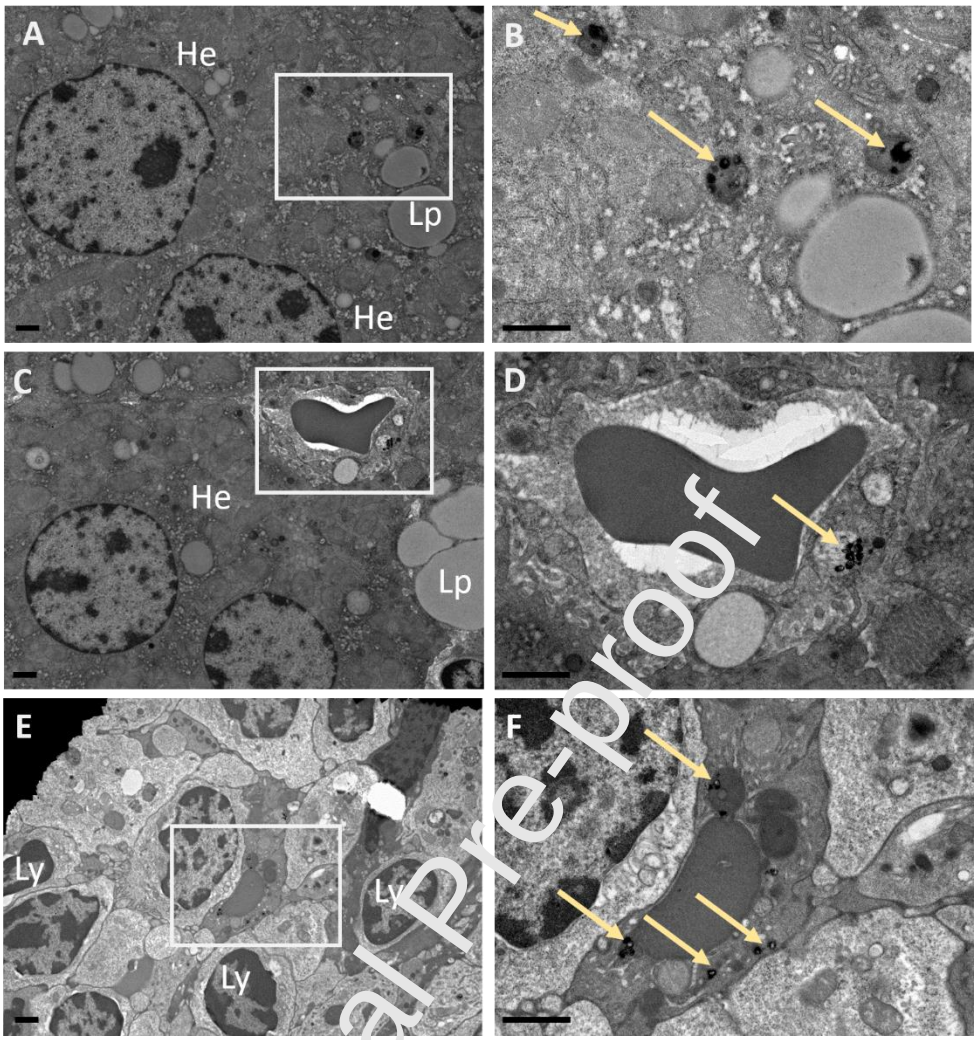


Figure 9 – Transmission Electron Microscopy (TEM) images of the liver (A, B, C and D) and the spleen (E and F) of mice 24 hours after intravenous injection of hybridosomes®. A, C and E represent cell architecture at low magnification. Ultrastructural details inside the white rectangles in A, C and E are imaged in B, D and F, respectively. Yellow arrows indicate the NP inside the cells. Abbreviations: Hepatocytes (He), Lipid globule (Lp), Lymphocyte (Ly). Scale bar: 1 µm.

Finally, it is interesting to summarize the encapsulation properties of hybridosomes® by comparing them with similarly structured nanovectors. In fact, there are relatively few examples of capsules whose walls are entirely or partly made of nanoparticles, and capable of encapsulation [59–63]. Regarding the encapsulation efficiency, it is straightforward to calculate that we can reach a mass percentage of 47% ($m_{dye}/m_{vesicle}$). In comparison, Nie reported a maximal loading of 18.4% for the encapsulation of a photosensibilizer (Ce6) into vesicles made from gold NP [62] and of 28% for doxorubicin into iron oxide vesicles[63], using NP tethered with amphiphilic block-copolymers. In both cases, the encapsulation of the water-soluble drug is operated *via* the film rehydration method, an aqueous solution of the cargo being used as the solvent for the rehydration process. Lecommandoux et al reported a slightly higher load (34%) of an hydrophobic form of doxorubicin in the membrane of magnetic polymersomes, using a coprecipitation method [61]. The core encapsulation of hydrophobic drugs such as indomethacin or protonated ibuprofen in capsules made from Pickering emulsion is also reported, with relatively low loading efficiency (6%)[59,64]. This quantitative comparison of mass encapsulation rates ($m_{dye}/m_{vesicle}$) is questionable, as it varies

greatly with the density of the NP used (e.g. AuNP vs SPION), the proportion of polymer in the shell or the presence of an oil core in the case of Pickering emulsions. However, our results clearly show an unprecedented loading, thanks to the nanoprecipitation of the hydrophobic cargo within the core of the capsules.

**Conclusion**

The results presented here lift the veil on the mechanism of encapsulation in hybridosomes®, using the Ouzo effect. The essential result of this study is that we were able to encapsulate the model cargo in nanocapsules up to 170 g.$L^{-1}$, or equivalently 450 000 molecules/capsule. Thanks to the specific emission properties of the model cargo, we could monitor its physical state throughout the encapsulation process and provide a detailed mechanism. We show that this exceptional loading ability is specific to the Ouzo effect, since it generates at the same time the accumulation of the cargo in the Ouzo droplets and the formation of capsules around the droplets. This procedure is also extremely straightforward to implement.

Thanks to *in vitro* and *in vivo* fluorescence experiments, we were able to observe the cellular internalization of the cargo, after incubation with cells, and prove its availability in solution or after body injection. It is clear that the cargo (encapsulated under the form of a nanoprecipitate) can dissolve, leak out across the hybridosome® shell and transfer to any lipophilic compartment, such as liposomes membrane or body fat. Note that the controlled release of the drug may be achieved by adding additional polymer layers, but this is beyond the scope of this study.

This exceptional encapsulation method can be applied both to capsules made only of polymers and to hybridosomes®. In the case of hybridosomes®, the intrinsic properties of nanoparticles can add significant value. For example, the SPION used here ease the purification of the nano-carriers by magnetic separation, and allow electron microscopy observation and MRI monitoring. The use of gold nanoparticles seems also very promising in combination with the encapsulation of an anti-cancer molecule, for treatments combining radiotherapy and chemotherapy, for example in the case of glioblastoma. Work is in progress in this direction.

**Acknowledgements**

We are very grateful to M. Ciancone and F. Camerel for providing the liposomes, and to B. Lefeuvre for ICP measurements. We thank the staff of Animal Facility of Rennes (ARCHE / BIOSIT, Université de Rennes 1) for animal husbandry and care. This work was supported by the CNRS, the University Rennes 1, the Région Bretagne, and the University of Rennes 1, CNRS, INSERM UMS BIOSIT, Rennes, France.

**MATERIALS & METHODS**

***Materials.*** Superparamagnetic iron oxide NP (SPION) ($\gamma$-$Fe_2O_3$; mean diameter 5 nm) were synthesized following a reported procedure [38]. 4,4-Difluoro-8-(4-trimethylsilylethynylphenyl)-1,3,5,7-tetramethyl-2,6-diethyl-4-bora-3a,4a-diaza-s-indacene **1** (BODIPY, M = 476.2 g.mol$^{-1}$) was synthesized following a reported procedure [65]. Poly(ethylene glycol)-*b*-Poly(acrylic acid) ($M_{PEG}$ = 2 kDa; $M_{PAA}$ = 7.2 kDa) were kindly provided by G. Casterou. Tetrahydrofuran (GPR Rectapur ≥99% stabilized) was purchased from VWR and used as received. Samples were made using MilliQ water (18.2 MΩ.cm$^{-1}$).

***Elaboration of BODIPY-loaded hybridosomes®.*** Dye-loaded hybridosomes® were prepared by an implementation of the previously published procedure for the preparation of hollow hybridosomes® [32]. In a typical experiment, water was added to a THF solution containing dye **1** to reach THF/water 25/75. The final $Fe_2O_3$ concentration was in the range 10 – 50 µg.mL$^{-1}$. The PEG-PAA was then added at a concentration of 25 µmol.L$^{-1}$ ([acrylic acid units] = 2.4 mmol.L$^{-1}$). After a quick homogenization, the solvent was slowly evaporated overnight at 40°C. Two 24h magnetic separation were performed, the supernatant was discarded and the purified hybridosomes® were redispersed in fresh water. The hybridosomes® suspension was characterized by NTA (*vide infra*) and TEM using a Jeol 1400 electron microscope equipped with a Gatan Orius 1000 camera.

***Nanoparticle tracking analysis (NTA).*** The size distribution (hydrodynamic diameter) and particle concentration was determined by NTA. NTA was carried out with a Nanosight LM10 device system (Malvern Panalytical) equipped with a 40 mW laser working at λ = 638 nm. Video sequences were recorded via a CCD camera operating at 30 frames per second and evaluated via the NANOSIGHT NTA 2.0 Analytical Software Suite. A blank NTA measurement with pure water was performed to exclude a possible contamination with scatterers. For each sample, 3 acquisitions with an acquisition time of 60 s were performed at 25°C. Calculations of the hydrodynamic diameters were achieved taking the viscosity of water at the temperature of measurement.

***Titration of nanoprecipitated BODIPY in water.*** The nanoprecipitated BODIPY **1** was prepared by evaporating THF from THF/water (25/75) solutions of BODIPY. Then the suspensions were centrifuged (20 min, 3820 g, Mikro 220R - Hettich). The supernatant was extracted twice with dichloromethane, the organic phase was evaporated and re-dissolved in THF. The pellet was directly re-dissolved in THF. The titration of BODIPY in THF is performed by absorbance measurements ($\lambda_{max}$ = 526 nm) based on a calibration curve in the range [0.5;20] µmol.L$^{-1}$ BODIPY.

The nanoprecipitation yield (*NY*) is calculated as follows:

$$NY\ (\%) = \frac{[BOD]_{pellet}}{[BOD]_{pellet} + [BOD]_{sup}} \times 100$$

where $[BOD]_{pellet}$ and $[BOD]_{sup}$ are the concentrations of BODIPY in the pellet and in the supernatant after centrifugation, respectively.

***Encapsulation efficiency.*** The encapsulation yield (*EY*) in hybridosomes® was determined using an absorbance microplate reader (FLUOstar Omega - BMG Labtech), following this typical procedure: in a 96 wells absorbance microplate, the absorbance of both pellets and supernatants obtained by magnetic separation were determined at $\lambda_{max}$ = 535 nm. The *EY* was calculated as follows:

$$EY\ (\%) = \frac{A_{pellet}}{A_{pellet} + A_{sup}} \times 100$$

where $A_{pellet}$ is the absorbance of the magnetically purified BODIPY-loaded hybridosomes® suspension and $A_{sup}$ is the absorbance of the supernatant.

The total internal volume of the hybridosomes® is calculated using the formula:

$$V = \sum n_i . \frac{4\pi}{3} {R_i}^3$$

Which is a sum over all the discrete size bins ($i$) containing each a number $n_i$ of particles of hydrodynamic radius $R_i$.

The internal concentration in hybridosomes® can be calculated from EY and NTA measurements as follows:

$$C_{in} = \frac{n_{tot} \times EY}{V}$$

where $n_{tot}$ stands for the total amount of dye molecules. Error bars correspond to the mean deviation from the trend curve.

***ICP-OES for determination of the iron concentration.*** Typically, the hybridosomes® were dissolved in nitric acid for one week under heating at 40°C. After appropriate dilution with milliQ water, the iron concentration was determined using an iCAP 7000 Series ICP-OES spectrometer (Thermo Scientific) under an argon flow, previously calibrated from 0 to 2 ppm Fe.

***COSMO-RS calculations:*** COSMO-RS calculations were performed using COSMOtherm (evaluation version). The Conductor-like Screening Model for Realistic Solvation (COSMO-RS), combines quantum chemical DFT calculations with statistical thermodynamics and allows for the prediction of a broad range of physico-chemical properties of molecules in solution including solubility. Calculation parameters were set as follow (T=25°C; $\Delta G_{fusion}$ estimated by software).

***Fluorescence of BODIPY in different environments.*** Emission spectra were recorded on a Fluorolog-3 fluorimeter (Horiba Jobin-Yvon). The measurements were performed at 90° from incident light in a 45 µL fluorescence quartz cuvette (Hellma Suprasil; path length 3x3 mm) at an excitation wavelength of 400 nm and the emission was recorded from 450 to 750 nm.

***In vitro release.*** The release kinetics of BODIPY in different environments was studied by incubating BODIPY-loaded hybridosomes® or nanodispersed BODIPY with liposomes (at different concentrations) or Fetal Bovine Serum (FBS). Typically, 50 µL of BODIPY-loaded hybridosomes® were incubated with 50 µL of a suspension of liposomes, and water was added to reach a total volume of 250 µL. The liposomes dispersions (10 mg/mL; 90 %wt eggPC; 10 %wt $PEG_{2000}$-DSPE; $Z_{av}$ = 72 ± 0.8 nm; PDI = 0.235) were kindly provided by F. Camerel (ISCR). For short-time fluorescence release in liposomes, the fluorescence intensity was monitored at 25°C using a FLUOstar Omega (BMG Labtech) microplate reader equipped with a 485 ± 6 nm excitation band-path filter and a 520 ± 5 nm emission band-path filter. For long-time release kinetics, the fluorescence intensity at 537 nm upon excitation at 480 nm was monitored for 8 days using a Fluorolog-3 fluorimeter (Horiba Jobin-Yvon).

In this particular case, the shell of the hybridosomes® was composed of SPION and QD (CdSe/ZnS Cytodiagnostics) emitting at 665 nm.

***Cell culture and confocal imaging.*** GL261 cells were cultured in DMEM medium (Dutscher, Brumath, France) supplemented with 10 % heat inactivated FBS (Dutscher) and 2 mM L-Glutamine (PanBiotech, Aidenbach, Bavaria, Germany) in 8-well chambered coverglass suitable for confocal microscopy (Nunc™ Lab-Tek™). Wells were seeded with 25000 cells/well and incubated with 10 µL of concentrated hybridosomes® ([Fe] ≈ 200 µg/mL) for 3 hours at 37°C 5% $CO_2$. The culture medium is replaced by 100 µL of imaging medium before the confocal imaging. Images were acquired with a LSM 880 confocal (Zeiss) equipped with a 63X oil-immersion objective (NA 1.4) driven by ZEN software. The excitation laser was set at 488 nm, the green emission channel detector at 517-544 nm and the orange emission channel detector at 579-624 nm. Images were analyzed and processed with ImageJ.

***In vivo release.*** For the release study in matrigel® (Growth Factor Reduced (GFR) matrigel®, Corning, Tewksbury, MA), one immunocompromized adult NSG mouse (NOD.*Cg-Prkdcscid Il2rgtm1Wjl/SzJ*; Charles River Laboratories, Wilmington, MA), anesthetized with inhaled isoflurane, was injected subcutaneously with matrigel® containing Nalm6 cells (i.e. 50 µL matrigel® mixed with 50 µL 1 million Nalm6 in PBS). After 9 days, 50 µL of BODIPY-loaded hybridosomes® were injected in the matrigel® and the fluorescence was monitored the following days, using a PhotonImager Optima bioimager (Biospace Lab, Nesles la Vallée, France) equipped with a highly sensitive cooled CCD camera. The same region of interest (ROI) was used for all the recordings in order to compare the intensities over time. For the systemic release study, two Balb/c nude mice (Charles River), anesthetized with isoflurane, were injected 50 µL of BODIPY-loaded hybridosomes® in the retro-orbital vein and the fluorescence was monitored over a week. The whole-mouse photon intensity was recorded. The mice were bred in the animal facility of the University of Rennes (Arche, BIOSIT) under SPF status and unsed at 6-12 weeks of age. These experiments were approved by the ethics committee for animal experimentation of the French Ministry for Higher Education and Scientific Research (Agreement A-35-238 40).

***Transmission Electronic Microscopy (TEM) of biological samples for in vivo biodistribution study.*** C57Bl/6 mice were intravenously injected with 50 µL of hybridosomes® (1 mg Fe/kg) and euthanized 24 h after the injection. After the dissection of the liver and the spleen, small pieces of tissues were fixed in 2.5% glutaraldehyde in cacodylate buffer during 1 hour at room temperature. Then, after 3 washes in cacodylate buffer, the samples were impregnated in heavy metal solution (1% osmium tetroxide) for 1 hour. Next, after rinsing, the samples were dehydrated with graded acetone series following standard procedures and embedded in Epon-Araldite-DMP30 resin (polymerized at 60°C for 48h). Ultrathin sections of 80 nm were cut (Leica UC7 ultramicrotome, Wetzlar, Germany), collected on copper grids, poststained with 2% uranyl acetate solution and finally imaged with a Jeol 1400 electron microscope (Jeol Co., Ltd, Tokyo, Japan) equipped with a Gatan Orius 1000 camera.

## References

[1] V. Đorđević, A. Paraskevopoulou, F. Mantzouridou, S. Lalou, M. Pantić, B. Bugarski, V. Nedović, Encapsulation Technologies for Food Industry, in: V. Nedović, P. Raspor, J. Levi ć, V. Tumbas Šaponjac, G.V. Barbosa-Cánovas (Eds.), Emerging and Traditional Technologies for Safe, Healthy

and Quality Food, Springer International Publishing, Cham, 2016: pp. 329–382. doi:10.1007/978-3-319-24040-4_18.
[2] Md. Saifullah, M.R.I. Shishir, R. Ferdowsi, M.R. Tanver Rahman, Q. Van Vuong, Micro and nano encapsulation, retention and controlled release of flavor and aroma compounds: A critical review, Trends in Food Science & Technology. 86 (2019) 230–251. doi:10.1016/j.tifs.2019.02.030.
[3] J. Riikonen, W. Xu, V.-P. Lehto, Mesoporous systems for poorly soluble drugs – recent trends, International Journal of Pharmaceutics. 536 (2018) 178–186. doi:10.1016/j.ijpharm.2017.11.054.
[4] U. Wais, A.W. Jackson, T. He, H. Zhang, Nanoformulation and encapsulation approaches for poorly water-soluble drug nanoparticles, Nanoscale. 8 (2016) 1746–1769. doi:10.1039/C5NR07161E.
[5] C. Ye, H. Chi, A review of recent progress in drug and protein encapsulation: Approaches, applications and challenges, Materials Science and Engineering: C. 83 (2018) 233–246. doi:10.1016/j.msec.2017.10.003.
[6] F. Casanova, L. Santos, Encapsulation of cosmetic active ingredients for topical application – a review, Journal of Microencapsulation. 33 (2016) 1–17. doi:10.3109/02652048.2015.1115900.
[7] K. Miyata, R.J. Christie, K. Kataoka, Polymeric micelles for nano-scale drug delivery, Reactive and Functional Polymers. 71 (2011) 227–234. doi:10.1016/j.reactfunctpolym.2010.10.009.
[8] C.J. Martínez Rivas, M. Tarhini, W. Badri, K. Miladi, H. Greige-Gerges, Q.A. Nazari, S.A. Galindo Rodríguez, R.Á. Román, H. Fessi, A. Elaissari, Nanoprecipitation process: From encapsulation to drug delivery, International Journal of Pharmaceutics. 532 (2017) 66–81. doi:10.1016/j.ijpharm.2017.08.064.
[9] C.I.C. Crucho, M.T. Barros, Polymeric nanoparticles: A study on the preparation variables and characterization methods, Materials Science and Engineering: C. 80 (2017) 771–784. doi:10.1016/j.msec.2017.06.004.
[10] C.I.C. Crucho, Stimuli-Responsive Polymeric Nanoparticles for Nanomedicine, ChemMedChem. 10 (2015) 24–38. doi:10.1002/cmdc.201402290.
[11] D.E. Discher, F. Ahmed, Polymersomes, Annual Review of Biomedical Engineering. 8 (2006) 323–341. doi:10.1146/annurev.bioeng.8.061505.095838.
[12] J.S. Lee, J. Feijen, Polymersomes for drug delivery: Design, formation and characterization, Journal of Controlled Release. 161 (2012) 473–483. doi:10.1016/j.jconrel.2011.10.005.
[13] A.F. Moreira, D.R. Dias, I.J. Correia, Stimuli-responsive mesoporous silica nanoparticles for cancer therapy: A review, Microporous and Mesoporous Materials. 236 (2016) 141–157. doi:10.1016/j.micromeso.2016.08.038.
[14] A. Wicki, D. Witzigmann, V. Balasubramanian, J. Huwyler, Nanomedicine in cancer therapy: Challenges, opportunities, and clinical applications, Journal of Controlled Release. 200 (2015) 138–157. doi:10.1016/j.jconrel.2014.12.030.
[15] M. Longmire, P.L. Choyke, H. Kobayashi, Clearance properties of nano-sized particles and molecules as imaging agents: considerations and caveats, Nanomedicine. 3 (2008) 703–717. doi:10.2217/17435889.3.5.703.
[16] F. Alexis, E. Pridgen, L.K. Molnar, O.C. Farokhzad, Factors Affecting the Clearance and Biodistribution of Polymeric Nanoparticles, Mol. Pharmaceutics. 5 (2008) 505–515. doi:10.1021/mp800051m.
[17] H. Soo Choi, W. Liu, P. Misra, E. Tanaka, J.P. Zimmer, B. Itty Ipe, M.G. Bawendi, J.V. Frangioni, Renal clearance of quantum dots, Nat Biotechnol. 25 (2007) 1165–1170. doi:10.1038/nbt1340.
[18] G. Chen, I. Roy, C. Yang, P.N. Prasad, Nanochemistry and Nanomedicine for Nanoparticle-based Diagnostics and Therapy, Chem. Rev. 116 (2016) 2826–2885. doi:10.1021/acs.chemrev.5b00148.
[19] Y. (Chezy) Barenholz, Doxil® — The first FDA-approved nano-drug: Lessons learned, Journal of Controlled Release. 160 (2012) 117–134. doi:10.1016/j.jconrel.2012.03.020.

[20] X. Wei, D. Shamrakov, S. Nudelman, S. Peretz-Damari, E. Nativ-Roth, O. Regev, Y. Barenholz, Cardinal Role of Intraliposome Doxorubicin-Sulfate Nanorod Crystal in Doxil Properties and Performance, ACS Omega. 3 (2018) 2508–2517. doi:10.1021/acsomega.7b01235.
[21] P.P. Wibroe, D. Ahmadvand, M.A. Oghabian, A. Yaghmur, S.M. Moghimi, An integrated assessment of morphology, size, and complement activation of the PEGylated liposomal doxorubicin products Doxil®, Caelyx®, DOXOrubicin, and SinaDoxosome, Journal of Controlled Release. 221 (2016) 1–8. doi:10.1016/j.jconrel.2015.11.021.
[22] T. Li, D. Cipolla, T. Rades, B.J. Boyd, Drug nanocrystallisation within liposomes, Journal of Controlled Release. 288 (2018) 96–110. doi:10.1016/j.jconrel.2018.09.001.
[23] E. Lepeltier, C. Bourgaux, P. Couvreur, Nanoprecipitation and the "Ouzo effect": Application to drug delivery devices, Advanced Drug Delivery Reviews. 71 (2014) 86–97. doi:10.1016/j.addr.2013.12.009.
[24] C.E. Mora-Huertas, H. Fessi, A. Elaissari, Influence of process and formulation parameters on the formation of submicron particles by solvent displacement and emulsification–diffusion methods: Critical comparison, Advances in Colloid and Interface Science. 163 (2011) 90–122. doi:10.1016/j.cis.2011.02.005.
[25] S.A. Vitale, J.L. Katz, Liquid Droplet Dispersions Formed by Homogeneous Liquid–Liquid Nucleation: "The Ouzo Effect," Langmuir. 19 (2003) 4105–4110. doi:10.1021/la026842o.
[26] I. Grillo, Small-angle neutron scattering study of a worldwide known emulsion: Le Pastis, Colloids and Surfaces A: Physicochemical and Engineering Aspects. 225 (2003) 153–160. doi:10.1016/S0927-7757(03)00331-5.
[27] N.L. Sitnikova, R. Sprik, G. Wegdam, E. Eiser, Spontaneously Formed trans-Anethol/Water/Alcohol Emulsions: Mechanism of Formation and Stability, Langmuir. 21 (2005) 7083–7089. doi:10.1021/la046816l.
[28] D. Carteau, I. Pianet, P. Brunerie, B. Guillemat, D.M. Bassani, Probing the Initial Events in the Spontaneous Emulsification of *trans*-Anethole Using Dynamic NMR Spectroscopy, Langmuir. 23 (2007) 3561–3565. doi:10.1021/la062339q.
[29] E. Scholten, E. van der Linden, H. This, The Life of an Anise-Flavored Alcoholic Beverage: Does Its Stability Cloud or Confirm Theory?, Langmuir. 24 (2008) 1701–1706. doi:10.1021/la702186g.
[30] X. Yan, P. Alcouffe, G. Sudre, L. David, J. Bernard, F. Ganachaud, Modular construction of single-component polymer nanocapsules through a one-step surfactant-free microemulsion templated synthesis, Chem. Commun. 53 (2017) 1401–1404. doi:10.1039/C6CC09701D.
[31] X. Yan, M. Remond, Z. Zheng, F. Hoibian, C. Soulage, S. Chambert, C. Andraud, B. Van der Sanden, F. Ganachaud, Y. Bretonnière, J. Bernard, General and Scalable Approach to Bright, Stable, and Functional AIE Fluorogen Colloidal Nanocrystals for in Vivo Imaging, ACS Appl. Mater. Interfaces. 10 (2018) 25154–25165. doi:10.1021/acsami.8b07859.
[32] F. Sciortino, G. Casterou, P.-A. Eliat, M.-B. Troadec, C. Gaillard, S. Chevance, M.L. Kahn, F. Gauffre, Simple Engineering of Polymer-Nanoparticle Hybrid Nanocapsules, ChemNanoMat. 2 (2016) 796–799. doi:10.1002/cnma.201600155.
[33] F. Sciortino, M. Thivolle, M.L. Kahn, C. Gaillard, S. Chevance, F. Gauffre, Structure and elasticity of composite nanoparticle/polymer nanoshells (hybridosomes®), Soft Matter. 13 (2017) 4393–4400. doi:10.1039/C7SM00705A.
[34] H. Jakobczyk, F. Sciortino, S. Chevance, F. Gauffre, M.-B. Troadec, Promises and limitations of nanoparticles in the era of cell therapy: Example with CD19-targeting chimeric antigen receptor (CAR)-modified T cells, International Journal of Pharmaceutics. 532 (2017) 813–824. doi:10.1016/j.ijpharm.2017.07.075.
[35] B.P. Binks, Particles as surfactants—similarities and differences, Interface Science. (2002) 21.
[36] K. Larson-Smith, D.C. Pozzo, Pickering Emulsions Stabilized by Nanoparticle Surfactants, Langmuir. 28 (2012) 11725–11732. doi:10.1021/la301896c.

[37] F. Sciortino, G. Rydzek, F. Grasset, M.L. Kahn, J.P. Hill, S. Chevance, F. Gauffre, K. Ariga, Electro-click construction of hybrid nanocapsule films with triggered delivery properties, Phys. Chem. Chem. Phys. 20 (2018) 2761–2770. doi:10.1039/C7CP07506E.
[38] G. Casterou, V. Collière, P. Lecante, Y. Coppel, P.-A. Eliat, F. Gauffre, M.L. Kahn, Improved Transversal Relaxivity for Highly Crystalline Nanoparticles of Pure γ-Fe2O3 Phase, Chemistry – A European Journal. 21 (2015) 18855–18861. doi:10.1002/chem.201502905.
[39] H. Inui, K. Itoh, M. Matsuo, J. Miyamoto, Studies on biodegradation of 2,6-di-tert-butyl-4-methylphenol (BHT) in the environment part-III Biodegradability of BHT with activated sludge, Chemosphere. 8 (1979) 383–391. doi:10.1016/0045-6535(79)90129-2.
[40] US EPA. 2020. Estimation Programs Interface Suite™ for Microsoft® Windows, v 4.11. United States Environmental Protection Agency, Washington, DC, USA, n.d.
[41] Z. Li, H. Cheng, J. Li, J. Hao, L. Zhang, B. Hammouda, C.C. Han, Large-Scale Structures in Tetrahydrofuran–Water Mixture with a Trace Amount of Antioxidant Butylhydroxytoluene (BHT), J. Phys. Chem. B. 115 (2011) 7887–7895. doi:10.1021/jp203777g.
[42] M. Hahn, S. Krickl, T. Buchecker, G. Jošt, D. Touraud, P. Bauduin, A. Pfitzner, A. Klamt, W. Kunz, Ab initio prediction of structuring/mesoscale inhomogeneities in surfactant-free microemulsions and hydrogen-bonding-free microemulsions, Phys. Chem. Chem. Phys. 21 (2019) 8054–8066. doi:10.1039/C8CP07544A.
[43] Y. Liao, V. Génot, R. Méallet-Renault, T.T. Vu, J.-F. Audibert, J.-P. Lemaistre, G. Clavier, P. Retailleau, R.B. Pansu, Spectroscopy of BODIPY in solid phase: crystal and nanoparticles, Phys. Chem. Chem. Phys. 15 (2013) 3186–3195. doi:10.1039/C2CP43289G.
[44] L. Wang, L. Li, D. Cao, A BODIPY-based dye with red fluorescence in solid state and used as a fluorescent and colorimetric probe for highly selective detection of cyanide, Sensors and Actuators B: Chemical. 239 (2017) 1307–1317. doi:10.1016/j.snb.2016.09.112.
[45] Y. Barenolz, G. Haran, Method of amphipathic drug loading in liposomes by pH gradient, US5192549A, 1993. https://patents.google.com/patent/US5192549A/en (accessed February 4, 2020).
[46] Mathematical models of drug release, in: Strategies to Modify the Drug Release from Pharmaceutical Systems, Elsevier, 2015. pp. 63–86. doi:10.1016/B978-0-08-100092-2.00005-9.
[47] R.W. Korsmeyer, R. Gurny, E. Doelker, P. Buri, N.A. Peppas, Mechanisms of solute release from porous hydrophilic polymers, International Journal of Pharmaceutics. 15 (1983) 25–35. doi:10.1016/0378-5173(83)90064-9.
[48] P.L. Ritger, N.A. Peppas, A simple equation for description of solute release I. Fickian and non-fickian release from non-swellable devices in the form of slabs, spheres, cylinders or discs, Journal of Controlled Release. 5 (1987) 23–36. doi:10.1016/0168-3659(87)90034-4.
[49] T. Szatmári, K. Lumniczky, S. Désaknai, S. Trajcevski, E.J. Hídvégi, H. Hamada, G. Sáfrány, Detailed characterization of the mouse glioma 261 tumor model for experimental glioblastoma therapy, Cancer Science. 97 (2006) 546–553. doi:10.1111/j.1349-7006.2006.00208.x.
[50] C.K. Kim, P. Ghosh, C. Pagliuca, Z.-J. Zhu, S. Menichetti, V.M. Rotello, Entrapment of Hydrophobic Drugs in Nanoparticle Monolayers with Efficient Release into Cancer Cells, J. Am. Chem. Soc. 131 (2009) 1360–1361. doi:10.1021/ja808137c.
[51] K. Kettler, K. Veltman, D. van de Meent, A. van Wezel, A.J. Hendriks, Cellular uptake of nanoparticles as determined by particle properties, experimental conditions, and cell type, Environmental Toxicology and Chemistry. 33 (2014) 481–492. doi:10.1002/etc.2470.
[52] L. Debaize, H. Jakobczyk, S. Avner, J. Gaudichon, A.-G. Rio, A.A. Sérandour, L. Dorsheimer, F. Chalmel, J.S. Carroll, M. Zörnig, M.A. Rieger, O. Delalande, G. Salbert, M.-D. Galibert, V. Gandemer, M.-B. Troadec, Interplay between transcription regulators RUNX1 and FUBP1 activates an enhancer of the oncogene c-KIT and amplifies cell proliferation, Nucleic Acids Res. 46 (2018) 11214–11228. doi:10.1093/nar/gky756.

[53] M.O. Durymanov, A.A. Rosenkranz, A.S. Sobolev, Current Approaches for Improving Intratumoral Accumulation and Distribution of Nanomedicines, Theranostics. 5 (2015) 1007–1020. doi:10.7150/thno.11742.
[54] L. Miao, L. Huang, Exploring the Tumor Microenvironment with Nanoparticles, in: C.A. Mirkin, T.J. Meade, S.H. Petrosko, A.H. Stegh (Eds.), Nanotechnology-Based Precision Tools for the Detection and Treatment of Cancer, Springer International Publishing, Cham, 2015: pp. 193–226. doi:10.1007/978-3-319-16555-4_9.
[55] B. Zhang, Y. Hu, Z. Pang, Modulating the Tumor Microenvironment to Enhance Tumor Nanomedicine Delivery, Front. Pharmacol. 8 (2017) 952. doi:10.3389/fphar.2017.00952.
[56] N. Luciani, F. Gazeau, C. Wilhelm, Reactivity of the monocyte/macrophage system to superparamagnetic anionic nanoparticles, J. Mater. Chem. 19 (2009) 6373–6380. doi:10.1039/B903306H.
[57] B.E. Rabinow, Nanosuspensions in drug delivery, Nat Rev Drug Discov. 3 (2004) 785–796. doi:10.1038/nrd1494.
[58] X. Li, Wang, Wang, Xu, Cheng, Wei, Formulation and pharmacokinetic evaluation of a paclitaxel nanosuspension for intravenous delivery, IJN. (2011) 1497. doi:10.2147/IJN.S21097.
[59] S. Simovic, H. Hui, Y. Song, A.K. Davey, T. Rades, C.A. Prestidge, An oral delivery system for indomethicin engineered from cationic lipid emulsions and silica nanoparticles, Journal of Controlled Release. 143 (2010) 367–373. doi:10.1016/j.jconrel.2010.01.008.
[60] E. Amstad, J. Kohlbrecher, E. Müller, T. Schweizer, M. Textor, E. Reimhult, Triggered Release from Liposomes through Magnetic Actuation of Iron Oxide Nanoparticle Containing Membranes, Nano Lett. 11 (2011) 1664–1670. doi:10.1021/nl200499.
[61] C. Sanson, O. Diou, J. Thévenot, E. Ibarboure, A. Soum, A. Brûlet, S. Miraux, E. Thiaudière, S. Tan, A. Brisson, V. Dupuis, O. Sandre, S. Lecommandoux, Doxorubicin Loaded Magnetic Polymersomes: Theranostic Nanocarriers for MR Imaging and Magneto-Chemotherapy, ACS Nano. 5 (2011) 1122–1140. doi:10.1021/an102762f.
[62] J. Lin, S. Wang, P. Huang, Z. Wang, S. Chen, G. Niu, W. Li, J. He, D. Cui, G. Lu, X. Chen, Z. Nie, Photosensitizer-Loaded Gold Vesicles with Strong Plasmonic Coupling Effect for Imaging-Guided Photothermal/ Photodynamic Therapy, 7 (2013) 10.
[63] K. Yang, Y. Liu, Y. Liu, Q. Zhang, C. Kong, C. Yi, Z. Zhou, Z. Wang, G. Zhang, Y. Zhang, N.M. Khashab, X. Chen, Z. Nie, Cooperative Assembly of Magneto-Nanovesicles with Tunable Wall Thickness and Permeability for MRI-Guided Drug Delivery, J. Am. Chem. Soc. 140 (2018) 4666–4677. doi:10.1021/jacs.8b00824.
[64] P.M. Sy, N. Anton, Y. Idoux-Gillet, S.M. Dieng, N. Messaddeq, S. Ennahar, M. Diarra, T.F. Vandamme, Pickering nano-emulsion as a nanocarrier for pH-triggered drug release, International Journal of Pharmaceutics. 549 (2018) 299–305. doi:10.1016/j.ijpharm.2018.07.066.
[65] G. Ulrich, R. Ziessel, Convenient and Efficient Synthesis of Functionalized Oligopyridine Ligands Bearing Accessory Pyrromethene-BF2 Fluorophores, J. Org. Chem. 69 (2004) 2070–2083. doi:10.1021/jo035825g.

**Clement Goubault:** conceptualization, methodology, Investigation, Project administration Writing - Original Draft, Visualization; **Flavien Sciortino:** Conceptualization ; Investigation ; Writing - Review & Editing; **Olivier Mongin:** Resources; **Ulrich Jarry**: Investigation, Methodology, Resources; **Mégane Bostoën** : Investigation; **Hélène Jakobczyk:** Investigation; **Agnès Burel :** Investigation, Resources, Visualization; **Stephanie Dutertre :** Investigation, resources; **MB TRoadec:** Investigation; Writing -Review & Editing; **Myrtil L. Kahn:** Investigation, Resources, Writing -Review & Editing, Funding acquisition; **Soizic Chevance:** Conceptualization, Methodology, Writing - Review & Editing, Supervision, Project administration; **Fabienne Gauffre**: Conceptualization, Methodology, Writing - Original Draft, Supervision, Project administration; Funding acquisition.

Higlights

- The Ouzo effect enables high loading of Hybridosomes (hybrid capsule)
- The cargo is nanoprecipitated within the core of Hybridosomes
- The cargo is released to the body while the capsule is captured by the macrophages

Graphical abstract

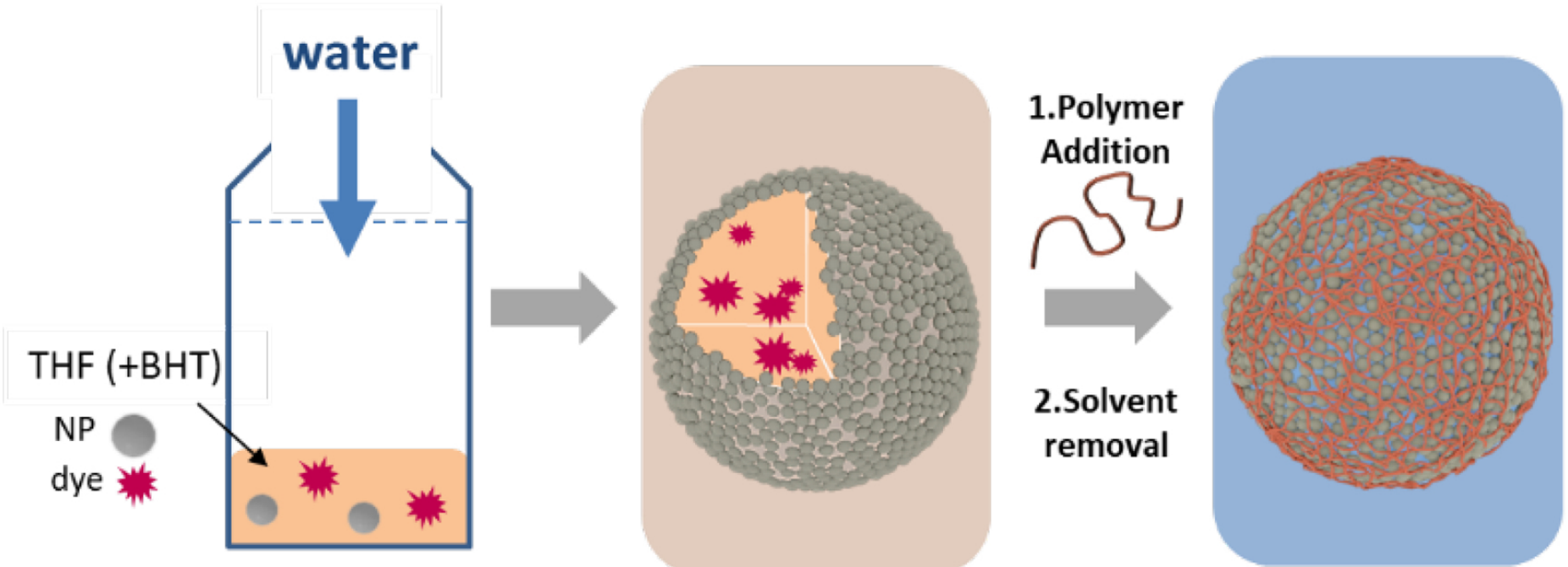


Figure 1

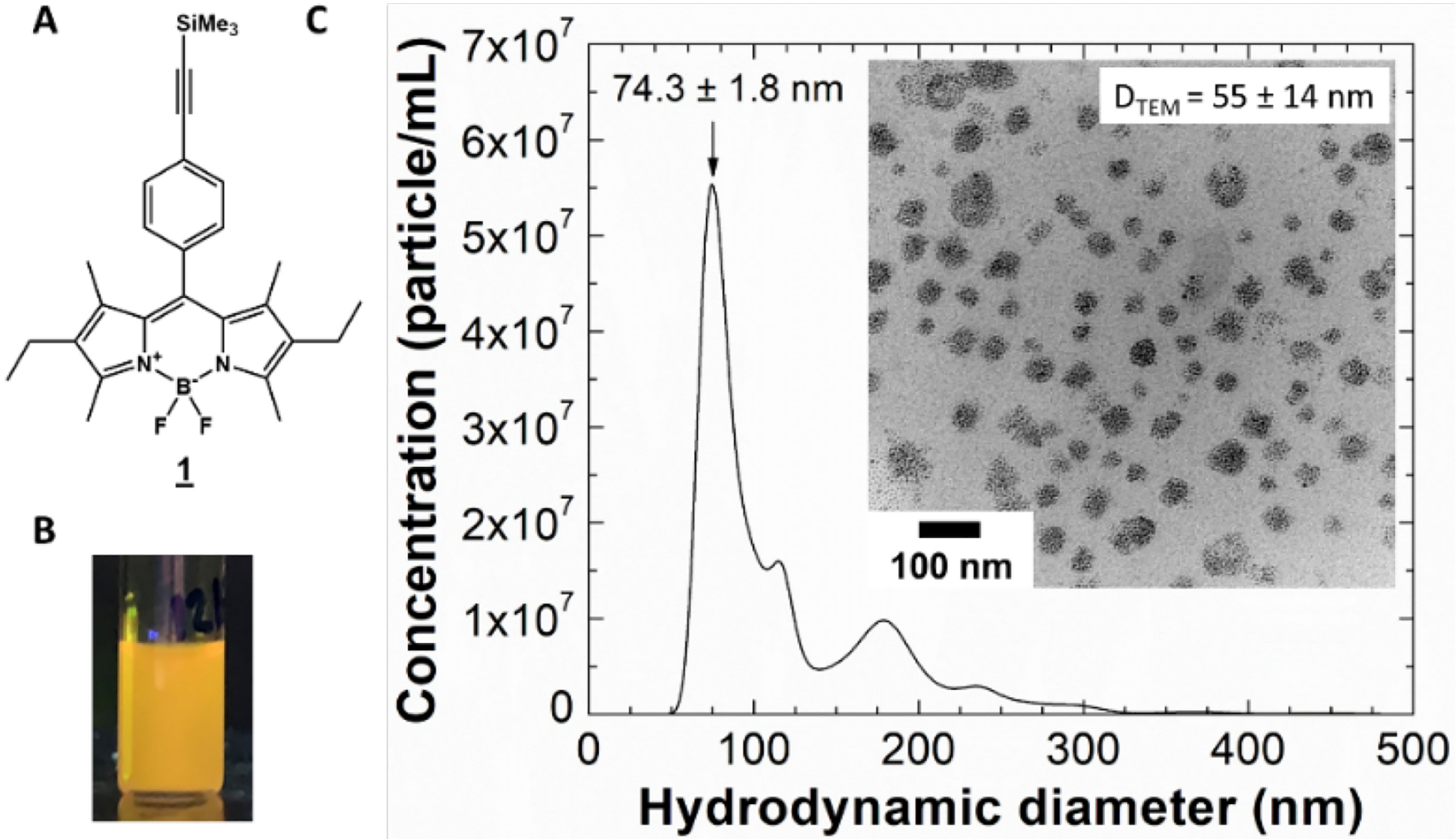
A
SiMe3
C
N+
B
N
F
F
1
B
Concentration (particle/mL)
7x10^7
6x10^7
5x10^7
4x10^7
3x10^7
2x10^7
1x10^7
0
74.3 ± 1.8 nm
D_TEM = 55 ± 14 nm
100 nm
0
100
200
300
400
500
Hydrodynamic diameter (nm)

Figure 2

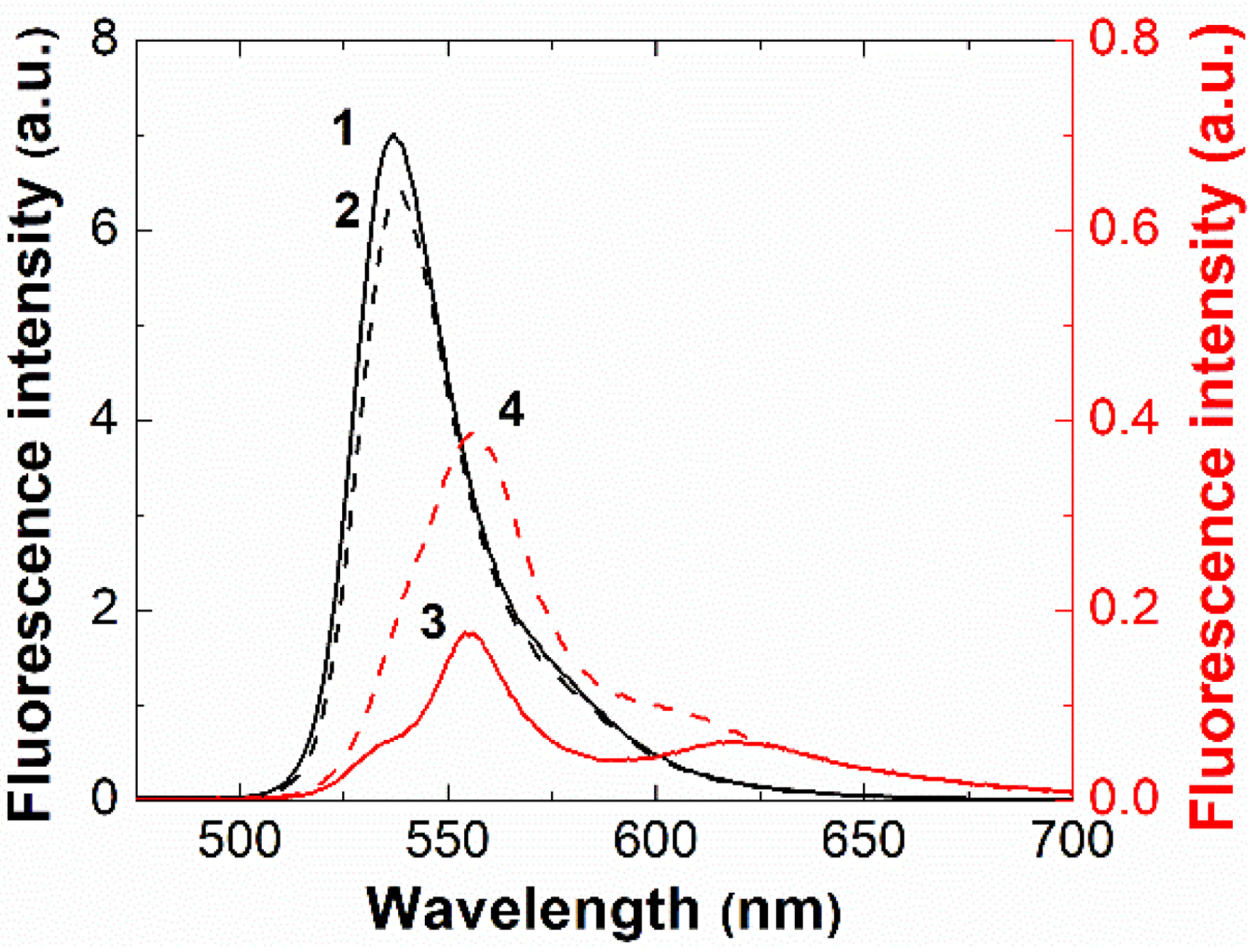
Fluorescence intensity (a.u.)
Fluorescence intensity (a.u.)
Wavelength (nm)
0
2
4
6
8
0.0
0.2
0.4
0.6
0.8
500
550
600
650
700
1
2
3
4

Figure 3

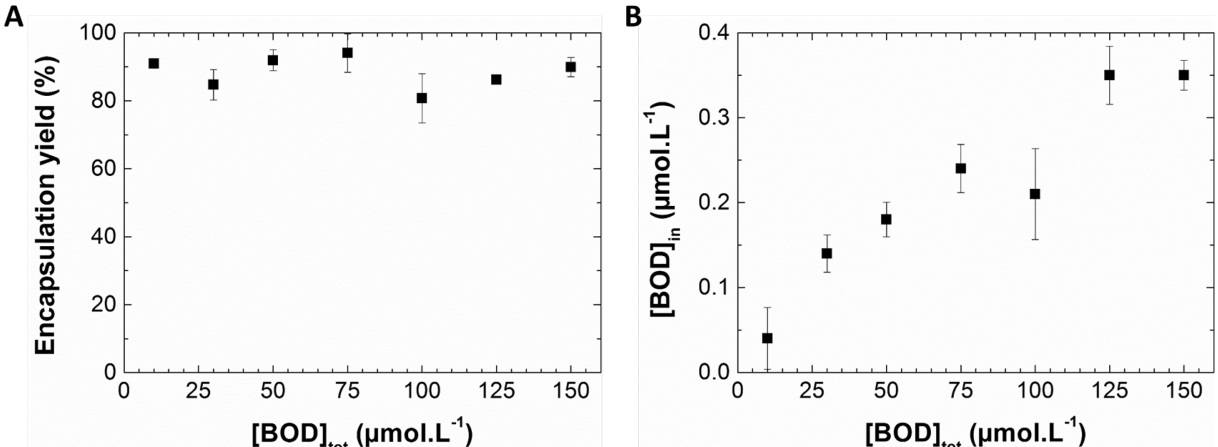
A
Encapsulation yield (%)
100
80
60
40
20
0
0
25
50
75
100
125
150
[BOD]tot (µmol.L-1)
B
[BOD]in (µmol.L-1)
0.4
0.3
0.2
0.1
0.0
0
25
50
75
100
125
150
[BOD]tot (µmol.L-1)

Figure 4

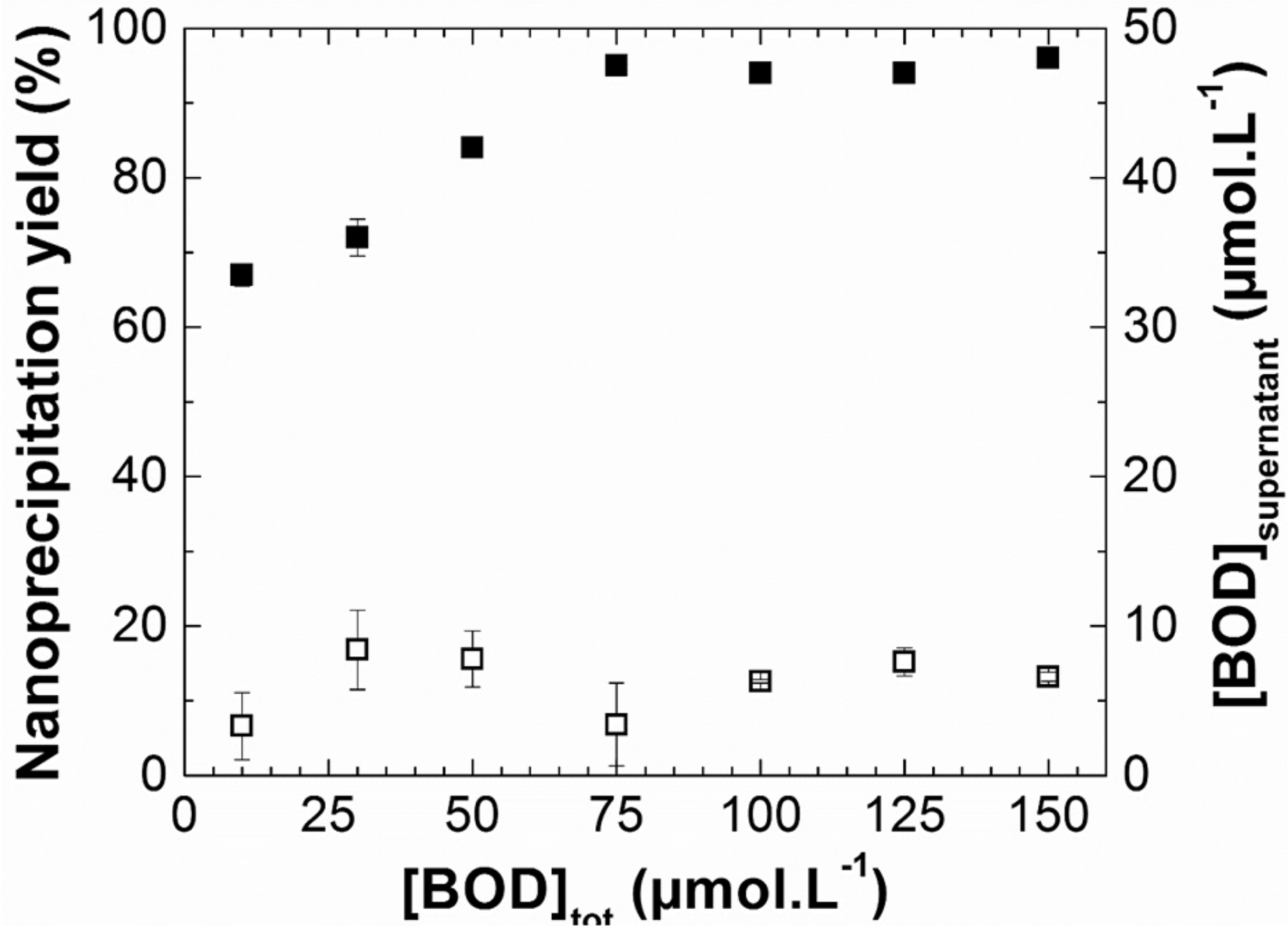
Nanoprecipitation yield (%)
100
80
60
40
20
0
0
25
50
75
100
125
150
[BOD]tot (µmol.L-1)
50
40
30
20
10
0
[BOD]supernatant (µmol.L-1)

Figure 5

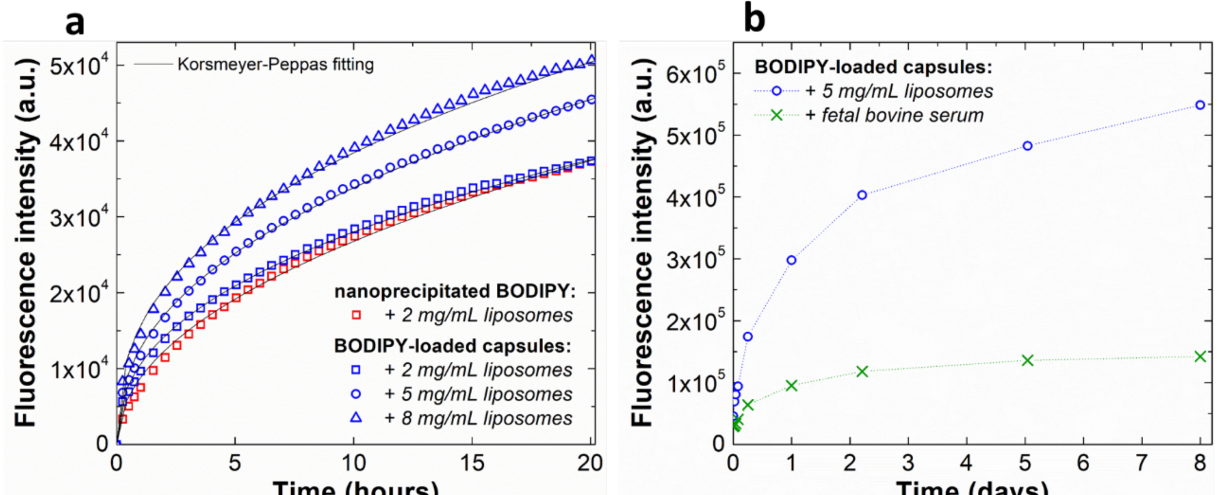
a
Fluorescence intensity (a.u.)
5x10^4
4x10^4
3x10^4
2x10^4
1x10^4
0
0
5
10
15
20
Time (hours)
Korsmeyer-Peppas fitting
nanoprecipitated BODIPY:
+ 2 mg/mL liposomes
BODIPY-loaded capsules:
+ 2 mg/mL liposomes
+ 5 mg/mL liposomes
+ 8 mg/mL liposomes
b
Fluorescence intensity (a.u.)
6x10^5
5x10^5
4x10^5
3x10^5
2x10^5
1x10^5
0
0
1
2
3
4
5
6
7
8
Time (days)
BODIPY-loaded capsules:
+ 5 mg/mL liposomes
+ fetal bovine serum

Figure 6

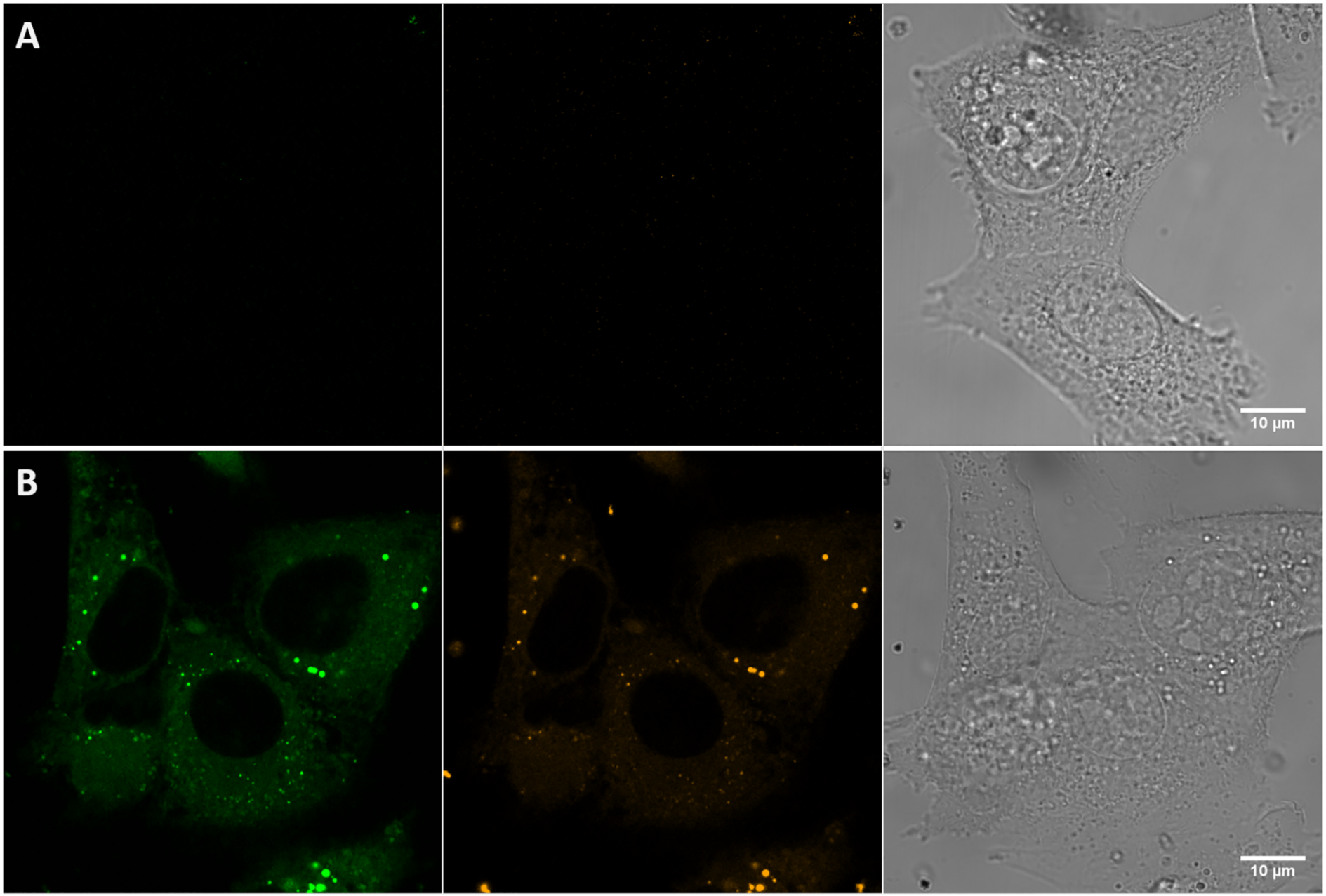


Figure 7

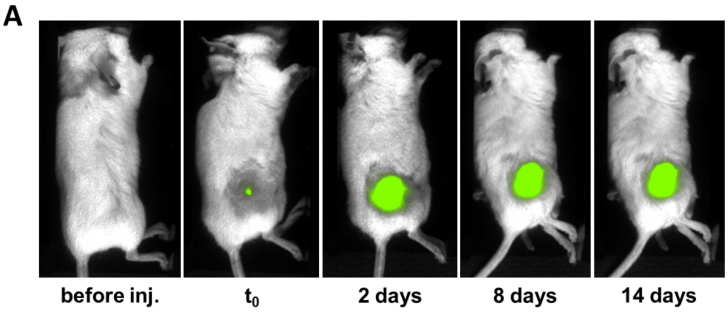
A
before inj.
$t_0$
2 days
8 days
14 days
B
Fluorescence intensity (a.u.)
0
5
10
15
20
25
0
2
4
6
8
10
12
14
Time after injection in matrigel (days)
C
50 min
1 day
2 days
5 days
D
Fluorescence intensity (a.u.)
0
100
200
300
400
0
1
2
3
4
5
Time after IV injection (days)

Figure 8

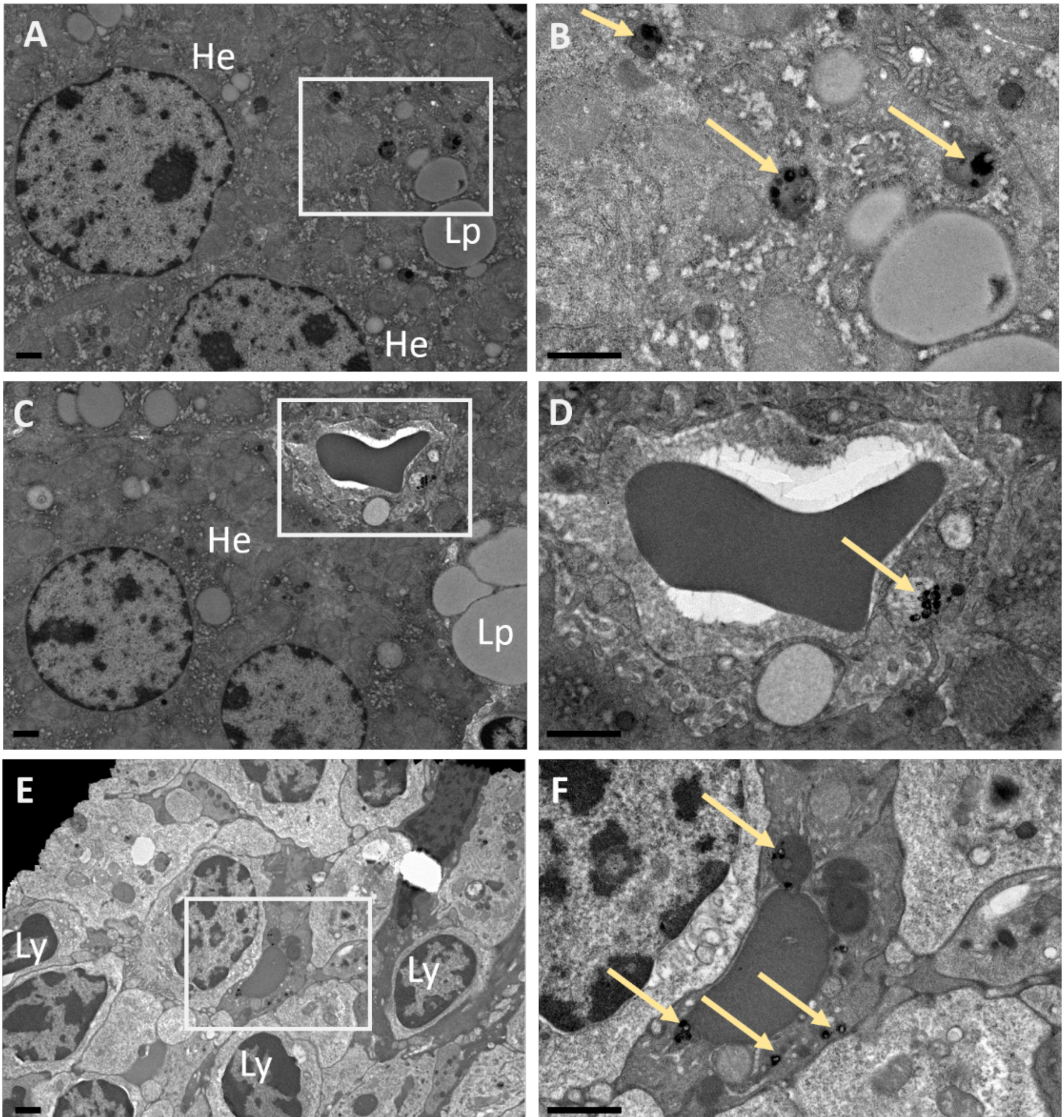


Figure 9